

# Robust Docking Maneuvers for Autonomous Trolley Collection: An Optimization-Based Visual Servoing Scheme

Yuhan Pang<sup>†</sup>, Bingyi Xia<sup>†</sup>, Zhe Zhang, Zhirui Sun, Peijia Xie, Bike Zhu, Wenjun Xu, and Jiankun Wang

**Abstract**—Service robots have demonstrated significant potential for autonomous trolley collection and redistribution in public spaces like airports or warehouses to improve efficiency and reduce cost. Usually, a fully autonomous system for the collection and transportation of multiple trolleys is based on a Leader-Follower formation of mobile manipulators, where reliable docking maneuvers of the mobile base are essential to align trolleys into organized queues. However, developing a vision-based robotic docking system faces significant challenges: high precision requirements, environmental disturbances, and inherent robot constraints. To address these challenges, we propose an optimization-based Visual Servoing scheme that incorporates active infrared markers for robust feature extraction across diverse lighting conditions. This framework explicitly models nonholonomic kinematics and visibility constraints within the Hybrid Visual Servoing problem, augmented with an observer for disturbance rejection to ensure precise and stable docking. Experimental results across diverse environments demonstrate the robustness of this system, with quantitative evaluations confirming high docking accuracy.

## I. INTRODUCTION

Mobile manipulation robots are revolutionizing automated transportation by taking over repetitive and heavy-load tasks from humans [1]–[3]. A promising application is the use of service robots to handle trolleys (i.e., carts), which are deployed in airports, shopping malls, and retail warehouses. These robots are expected to collect and redistribute trolleys after customer use (e.g., after shopping or airport departures) to improve operational efficiency and reduce costs. Specifically, multiple trolleys are required to be collected as a whole unit, and then transported to a designated destination. Through the cooperation of two robots, this task can be executed in a fully autonomous manner. As illustrated in Fig. 1, one robot pushes a trolley to dock with the other robot, iteratively stacking multiple trolleys into a complete queue.

This paper focuses on the docking maneuvers involved in the sequential stacking of multiple trolleys. This task imposes strict requirements on both robustness and precision, as misalignment and imperfect connection may lead to collision risks and operational failures. Our system is built on the dual-arm mobile robot proposed in [4]. They developed an adaptive arm controller for pushing trolleys, where mobile manipulation is decoupled into robot arm control and mobile base navigation. However, a gap remains in target localization and docking control when applying to the trolley stacking task. Currently, the arm controller regulates pushing forces according to the velocity of the mobile base; therefore, accurate docking maneuvers of the base are essential for adjusting the trolley’s pose. Furthermore, real-world deployment often encounters changing layouts and dense pedestrians, which

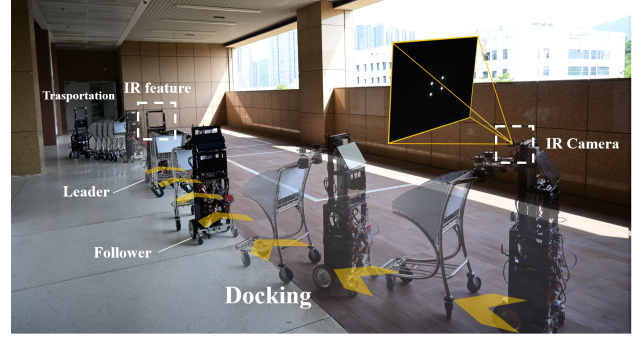


Fig. 1. The Follower robot docks the collected trolleys into an organized queue then transport them to designated location. Utilizing visual servoing, it achieves precise docking by observing the infrared features on the Leader robot through its onboard camera.

prevents reliance on ideal external infrastructure such as pre-built high-precision maps or wireless communication. Unlike conventional navigation tasks, the availability of methods based on global localization and path planning is severely limited in this scenario. Consequently, it is still challenging to achieve millimeter-level docking accuracy relying solely on the onboard camera.

Visual Servoing (VS) offers a promising solution by directly using visual feedback to guide the docking maneuvers [5]. Although basic VS approaches have been applied to other docking tasks [6], [7], they typically assume ideal pose estimation (e.g., AprilTag [8]) and do not account for process noise introduced by pushing a trolley. Our system presents a tightly coupled nonlinear control problem involving nonholonomic constraints, field-of-view (FOV) limitations, and dynamic disturbances. In addition, the system needs to remain robust in complex environments and long-term operation, facing challenges such as variable lighting, reflective surfaces (e.g., glass walls), and changing layouts. To deal with the dynamics complexity and environmental uncertainties inherent in the trolley collection task, existing VS-based docking requires improvements in two aspects: (1) robust visual feature extraction and state estimation, and (2) docking controller for accurate convergence under constraints.

To address the aforementioned challenges in trolley collection, we introduce a VS scheme for a docking system that operates solely on a monocular camera, without global localization in the world frame or inter-robot communication. To ensure robust perception, an active infrared (IR) marker array is equipped on the Leader robot, facilitating consistent and accurate visual feature extraction by the Follower robot. For the docking control of the Follower robot, a Nonlinear

Model Predictive Control (NMPC) approach is designed that explicitly accounts for the nonholonomic motion constraints of the mobile base while ensuring FOV constraints. Within the Hybrid VS scheme, the optimization problem is constructed using depth and orientation measurement, and is augmented with an extended state observer that significantly enhances robustness against perceptual noise and dynamic disturbances. Extensive real-world experiments validate the precision of the proposed approach. The main contributions of this paper are summarized as follows:

- We present a dual-robot system with specialized manipulators for trolley collection, featuring precise docking maneuvers based solely on monocular vision. Experiments across diverse real-world environments demonstrate the effectiveness and robustness of our system.
- A Hybrid VS scheme is introduced to achieve docking maneuvers under the nonholonomic constraints. For state measurement, we design an active infrared marker array as the visual feature, ensuring robust perception under variable lighting conditions.
- To solve the VS problem in real-time while maintaining feature visibility, we propose an optimization-based visual predictive controller, incorporating an extended state observer for disturbance rejection.

## II. RELATED WORK

Recent developments in mobile manipulation have emphasized the importance of human-like pushing skills for expanding payload capacity and service delivery [1], [2]. For trolley collection, previous studies have investigated trolley identification [3], dual-arm mobile manipulation [4], and collaborative queue transportation [9]. However, they heavily rely on global localization and navigation based on LiDAR and inter-robot communication, which are not always available in practice. For trolley stacking solely using onboard camera, this paper extends the previous system [4] with accurate docking maneuvers, thereby facilitating rapid deployment while ensuring low cost and system flexibility.

Docking is a critical capability for robots, referring to the maneuver of aligning a robot to a target with the desired position and orientation. It has been widely studied in logistics [10], [11], quadrotors [7], [12] and surface vehicles [13]. Path-tracking methods [14]–[16] rely on high-precision global localization and wireless communication for target pose estimation. In contrast, recent studies [6], [7], [17] have leveraged VS to reduce dependency on external modules, thereby developing lightweight systems using cameras. For mobile robot docking, Wang et al. [6] present a VS controller using AprilTag for target pose estimation. However, the docking problem in trolley stacking faces additional challenges involving model uncertainty and environmental limitations.

A basic VS scheme comprises two essential components: designing visual features associated with the target object and developing a control law to drive the convergence of feature errors. Visual features are generally defined as geometric primitives (e.g., points and lines). Recent efforts

have explored deep learning-based keypoint detection to improve accuracy and adaptability [18]. However, learning-based methods rely on training data and can be compromised under poor lighting. To adapt to diverse environments, recent studies on marker-based techniques propose using an active infrared or ultraviolet LED array, such as a circular fiducial marker [19]. In addition, CREPES [20] integrates UWB to enhance relative pose estimation with depth signal. Based on these studies, we develop active IR markers as reliable point features of VS-based docking.

VS approaches are traditionally classified into Position-based Visual Servoing (PBVS) and Image-based Visual Servoing (IBVS) depending on how they associate the image space with motion space [21]. PBVS defines control errors by the pose of the camera relative to the target, while IBVS directly controls the movement of visual features to the target frame. Hybrid VS [22], [23] combines both methods and extends the error state of the visual features using a pose estimation reference, thereby achieving improved performance. Recent advancements have further incorporated Hybrid VS into Model Predictive Control (MPC) [24]–[26], which is featured by long-horizon trajectory planning and optimization techniques. This scheme is particularly effective for underactuated systems while maintaining visibility of visual features. For nonholonomic robots, Ke et al. [24] proposed a MPC approach achieving position control through a single point-feature observation. Jin et al. [26] improve the orientation error convergence, despite their Gaussian process observer for model uncertainty also induces control signal fluctuation. Crucially, these approaches neglect practical orientation measurement and depend on the wheel odometry, thus treating depth measurement as unreliable.

Inspired by these insights, we address the docking problem in trolley collection by a Hybrid VS scheme. Our system leverages the geometric prior of the markers to provide both depth and orientation estimation, extending the error formulation beyond traditional IBVS. To improve robustness, we integrate an observer that filters the estimated state, effectively compensating for model uncertainty and process noise introduced by pushing the trolley.

## III. SYSTEM OVERVIEW

We introduce a robotic system as a Leader-Follower formation comprising two mobile manipulators for stacking multiple trolleys, which is shown in Fig. 1. The Follower is in charge of grasping and pushing trolleys, while the Leader, positioned at the head of the trolley queue, serves as the base for docking. The proposed pipeline that tightly couples with the robotic system is illustrated in Fig. 2.

The Follower robot utilizes dual Selective Compliance Assembly Robot Arms (SCARA) to stably push the trolley. Each robotic arm comprises three joint motors and a gripper. Both arms share a coaxial base mounted on a lead screw module for vertical adjustment. To effectively manipulate a trolley, the robot typically applies pushing forces along constrained directions by grasping the handle. Based on the adaptive low-level controller proposed in [4], the Follower

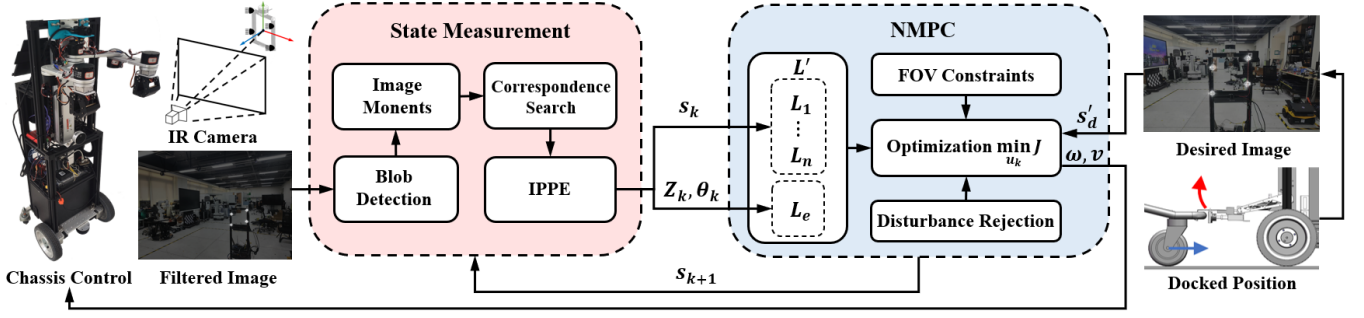


Fig. 2. Pipeline for docking process in trolley collection, which follows the optimization-based Hybrid VS scheme.

robot computes the joint torques of the arms to steer the trolley along the moving direction of the chassis.

During the docking process, the Follower robot uses its onboard monocular camera to perceive its state, where robot motion correlates with visual feature changes in image space. The target state is defined by a reference image captured at the docked position, depicting the relative pose between robots as perceived by the Follower's camera. Visual features are the image projections of an active infrared LED array (940 nm wavelength) mounted on the Leader robot, which are extracted through image processing. This human-invisible spectrum effectively minimizes light pollution in public environments. Correspondingly, a narrowband filter is placed between the camera lens and the CMOS sensor on the Follower, which transmits only this specific wavelength of light to produce high-contrast images.

The docking controller calculates the Follower's chassis velocity to achieve the docking formation as the current image converges to the desired image. Our visual predictive control approach comprises two components: state measurement and NMPC. First, the current filtered image from the Follower's camera is processed by morphological segmentation and image moment analysis. Leveraging the geometric prior of the LED configuration, the system establishes 2D-3D correspondences to solve for relative rotation and depth. This enables a Hybrid VS scheme that integrates the image interaction matrix with an extended depth-rotation relation matrix for state prediction. We formulate an online optimization problem considering external disturbances and system constraints to output velocity commands while using predicted feature motion for future correspondence matching. Subsequent sections provide details of the methodology.

The Follower determines the termination of the docking by the joint torque variations of its arm and the visual servoing error. Upon reaching the docking position, the Follower steers the trolley forward until all trolleys in the queue are rigidly connected. Notably, for docking with the first trolley, a gravity-based self-locking guide structure is designed as the end effector of the Leader robot. When the trolley's front beam contacts this guide structure, the front beam exerts a force along the direction of motion. In response, the guide structure generates a perpendicular reaction force (normal to the ground), which passively lifts the end effector. As the

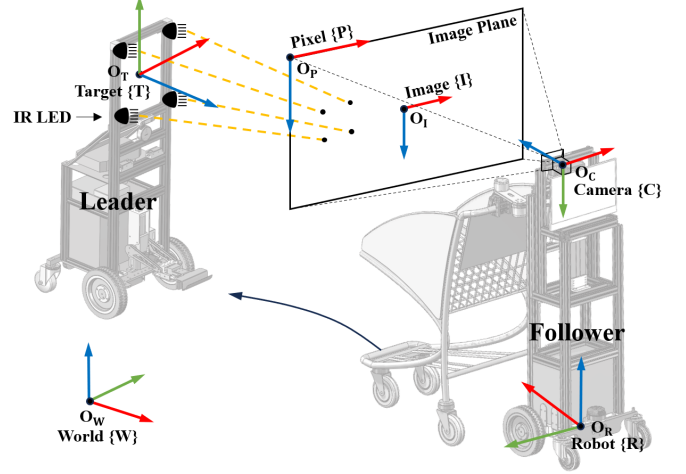


Fig. 3. Coordinate system description for robot docking process.

trolley moves further, the end effector first descends under gravitational force, then a linear actuator engages to securely lock the trolley's front beam.

## IV. PROBLEM FORMULATION

### A. Notations

The mathematical notation in this work follows these conventions: vectors and matrices are represented in boldface (e.g.,  $s$  for vectors and  $K$  for matrices), while sets are denoted using calligraphic font (e.g.,  $\mathcal{B}$ ). The transpose operation is indicated by  $^\top$  (e.g.,  $s^\top$ ). The  $[n]$  and  $[n]_\times$  are the symmetric and antisymmetric matrices associated with vector  $n$ . Additionally, superscripts are employed to specify reference frames, such as  $t_C^R$  representing the translation vector of frame  $\{C\}$  with respect to frame  $\{R\}$ .

The coordinate frames employed in the formulation are enumerated below and illustrated in Fig. 3:

- 1) Robot Frame  $\{R\}$ : Fixed on the chassis of the Follower robot, velocity commands are expressed in this frame.
- 2) Target Frame  $\{T\}$ : Centered at the IR marker array, representing the spatial configuration of the LEDs.
- 3) Camera Frame  $\{C\}$ : Attached to the camera at its optical center, with the Z-axis along the optical axis.
- 4) Pixel Frame  $\{P\}$ : With its origin at the image's top-left corner, marker projections are captured in this frame.
- 5) Image Frame  $\{I\}$ : Normalized image plane coordinates, which facilitate the derivation of the state equation.



### B. Preliminary

The differentially driven mobile robot follows the unicycle model with control input  $\mathbf{u}_R = [v_R, \omega_R]^\top$ , consisting of linear velocity and angular velocity:

$$\dot{x}_R = v_R \cos \theta_R, \quad \dot{y}_R = v_R \sin \theta_R, \quad \dot{\theta}_R = \omega_R, \quad (1)$$

where  $[x_R, y_R]^\top$  denotes the Cartesian coordinates on  $XOY$  plane, and  $\theta_R$  denotes the heading angle of robot. The position of Follower robot in target frame  $\{T\}$  is  $[x_R^T, y_R^T, z_R^T]^\top$ , where  $y_R^T$  is a constant due to the fixed installation of the marker. Note that although this coordinate is defined, the relative position is not explicitly computed in the subsequent methodology, but rather serves as the evaluation metric.

The relationship between the camera body velocity  $\nu_C = [v_C, \omega_C]^\top \in \mathbb{R}^6$  and the robot body velocity  $\nu_R$  is:

$$\nu_R = \mathbf{X}_C^R \nu_C, \quad \mathbf{X}_C^R = \begin{bmatrix} \mathbf{R}_C^R & [t_C^R] \mathbf{R}_C^R \\ \mathbf{0}_{3 \times 3} & \mathbf{R}_C^R \end{bmatrix}. \quad (2)$$

Let  $\mathbf{n}, \theta$  be the rotation axis and angle of the camera. The time derivative of  $\mathbf{n}\theta$  can be expressed as a function of the camera angular velocity:

$$\frac{d(\mathbf{n}\theta)}{dt} = \left[ \mathbf{I}_3 - \frac{\theta}{2} [\mathbf{n}]_\times + \left( 1 - \frac{\text{sinc}(\theta)}{\text{sinc}^2 \frac{\theta}{2}} \right) [\mathbf{n}]_\times^2 \right] \omega_C. \quad (3)$$

Based on the pinhole camera model, the projection relationship between a homogeneous pixel coordinate  $\mathbf{h} = [u, v, 1]^\top$  in frame  $\{P\}$  and a point  $\mathbf{P}^C = [X, Y, Z]^\top$  in frame  $\{C\}$  is given by:

$$\mathbf{Z}\mathbf{h} = \mathbf{K}\mathbf{P}^C, \quad (4)$$

where  $\mathbf{K} \in \mathbb{R}^{3 \times 3}$  is the camera intrinsic matrix. To simplify the notation related to image, we use  $\mathbf{p} = [u, v]^\top$  to denote the coordinates in frame  $\{P\}$  and  $\mathbf{s} = [x, y]^\top = [X/Z, Y/Z]^\top$  to denote the coordinates in frame  $\{I\}$ .

### C. Visual Servoing Docking Problem

Since VS is based on the relationship between camera velocity and feature motion, we take the time derivative of  $\mathbf{s}$  to obtain:

$$\dot{\mathbf{s}} = \begin{bmatrix} \dot{x} \\ \dot{y} \end{bmatrix} = \begin{bmatrix} (\dot{X} - x\dot{Z})/Z \\ (\dot{Y} - y\dot{Z})/Z \end{bmatrix}. \quad (5)$$

Define the image feature error as  $\mathbf{e} = \mathbf{s} - \mathbf{s}_d$ , with  $\mathbf{s}_d$  denoting the desired feature coordinates. Substituting the kinematics of a marker point in camera frame  $\{C\}$ :  $\mathbf{P}^C = -\mathbf{v}_C - \omega_C \times \mathbf{P}^C$  into (5), we obtain the interaction matrix  $\mathbf{L}$  such that:

$$\dot{\mathbf{e}} = \mathbf{L}\nu_C. \quad (6)$$

Thus, VS controls robotic motion by minimizing image feature error. When the visual features are sufficient, the robot's unique pose can be determined from the image. By treating the image observed at the docked position as the desired image, the robot docking problem is converted into a VS problem. However, directly defining the system state by feature coordinates may lead to local minima and steady-state error due to nonholonomic constraints. Motivated by Hybrid

VS in [22], we formulate the state as a combination of image coordinates, depth, and relative camera orientation:  $\mathbf{s}'(t) = [\mathbf{s}(t)^\top, Z(t), \theta(t)]^\top \in \mathbb{R}^{2n+2}$ , where  $n$  is the number of feature points. Correspondingly, the desired state is defined as  $\mathbf{s}'_d = [\mathbf{s}_d^\top, Z_d, 0]^\top$ , where  $\mathbf{s}_d$  is the feature coordinates when the robot is at desired docking pose,  $Z_d$  is the desired docking distance and the desired relative orientation is 0, representing alignment between the two robots.

Thus, the state error is obtained:  $\mathbf{e}'(t) = \mathbf{s}'(t) - \mathbf{s}'_d$ , and the control objective is to design  $\mathbf{u}_R(t)$  to drive the Follower robot to the desired docking state:

$$\lim_{t \rightarrow \infty} \|\mathbf{e}'(t)\| = 0. \quad (7)$$

### V. VISUAL PREDICTIVE DOCKING CONTROL

This section presents the proposed visual predictive control scheme, which comprises two components: state measurement and NMPC implementation.

#### A. State Measurement

For each captured image frame, a threshold  $\lambda_I$  is applied to the acquired grayscale image  $\mathbf{I}(u, v)$  to facilitate subsequent processing:

$$\mathbf{I}'(u, v) = \begin{cases} \mathbf{I}(u, v), & \text{if } \mathbf{I}(u, v) > \lambda_I \\ 0, & \text{otherwise.} \end{cases} \quad (8)$$

We perform blob detection and segmentation on  $\mathbf{I}'(u, v)$  and obtain a set of detected blobs  $\mathcal{B} = \{b_1, \dots, b_N\}$ , where each  $b_i$  represents a connected component in the thresholded image. We compute the centroid of each  $b_i$  with subpixel-level precision using image moments:

$$M_{pq}^i = \sum_{(u,v) \in b_i} u^p v^q \mathbf{I}'(u, v), \quad (9)$$

$$\mathbf{p}_i = [\hat{u}_i, \hat{v}_i]^\top = [M_{10}^i/M_{00}^i, M_{01}^i/M_{00}^i]^\top, \quad (10)$$

where  $p+q$  is the order of the image moments. This results in a set of candidate image points  $\mathcal{P} = \{\mathbf{p}_1, \dots, \mathbf{p}_N\}$  representing the centroids of the detected blobs. In complex lighting environments, interference may occur due to other devices emitting light in the same wavelength band. To identify valid IR marker projections among the detected points, we extract the marker set  $\mathcal{L} \subseteq \mathcal{P}$  by leveraging the spatial configuration and geometric constraints of the IR markers, while simultaneously recovering their correspondence.

Since the combinatorial point-matching method incurs high computational complexity when dealing with a large number of points, we instead establish a relationship between camera motion and the resulting optical flow of feature points. Based on (6), we predict the future feature coordinates at time  $t+1$  from the state at time  $t$ :  $\mathbf{s}_{t+1} = \mathbf{s}_t + \mathbf{L}\mathbf{u}_t/f_c$ , where  $f_c$  denotes camera frames per second (fps). Each detected feature point inherits the previous matching result if its distance to the nearest predicted point falls below a predefined threshold.

After the set  $\mathcal{L}$  is determined, the correspondence between points in the pixel frame  $\{P\}$  and points in the target



frame  $\{T\}$  is established, which constitutes a perspective-n-point problem. Based on the coplanar characteristic of the marker points, we employ the Infinitesimal Plane-Based Pose Estimation (IPPE) [27] method to compute the required state variables  $Z(t)$  and  $\theta(t)$ .

### B. NMPC Implementation

For a unicycle robot model with a horizontally mounted camera, the nonholonomic planar motion constraint reduces the camera velocity to  $\nu_C = [0, 0, v_z, 0, \omega_y, 0]^\top$  according to the transformation (2). This yields a compact interaction matrix for each point:

$$\mathbf{L} = \begin{bmatrix} x/Z & -(1+x^2) \\ y/Z & -xy \end{bmatrix}. \quad (11)$$

The depth update equation can be derived as:

$$\dot{Z} = -v_z + \omega_y X = -v_z + \omega_y x Z. \quad (12)$$

Since the prediction of feature points depends on  $Z$ , incorporating the depth as a state variable improves the accuracy of feature point prediction. The continuous-time system model is given by:

$$\dot{\mathbf{s}}' = \mathbf{L}' \mathbf{u}_C, \quad (13)$$

where  $\mathbf{s}' = [x_1, y_1, \dots, x_n, y_n, Z, \theta]^\top$  and  $\mathbf{u}_C = [v_z, \omega_y]^\top$  are the extended system state and camera velocity control input, respectively. The interaction matrix  $\mathbf{L}' \in \mathbb{R}^{(2n+2) \times 2}$  is defined with a block matrix structure:

$$\mathbf{L}' \triangleq [\mathbf{L}_1^\top \ \dots \ \mathbf{L}_n^\top \ \mathbf{L}_e^\top]^\top, \mathbf{L}_e \triangleq \begin{bmatrix} -1 & \hat{x}Z \\ 0 & 1 \end{bmatrix}, \quad (14)$$

where  $\mathbf{L}_1, \dots, \mathbf{L}_n$  are interaction matrices from (11),  $\mathbf{L}_e$  contains depth and orientation kinematics from (3) and (12), and  $\hat{x}$  is computed by averaging horizontal feature coordinates:  $\hat{x} = \sum_{i=1}^n x_i/n$ . By applying the forward Euler discretization with period  $T_s$ , we obtain the discrete-time prediction model as:

$$\mathbf{s}'_{k+1} = f(\mathbf{s}'_k, \mathbf{u}_k) = \mathbf{s}'_k + T_s \mathbf{L}' \mathbf{u}_k, \quad (15)$$

where  $\mathbf{s}'_k, \mathbf{u}_k$  represent the system state and control input at time step  $k$ , respectively.

Due to disturbances caused by orientation measurement errors and force exerted by the arm, a nonlinear extended state observer is introduced to treat the total system disturbance as an additional state for real-time estimation and compensation, without requiring precise prior knowledge of the disturbance dynamics. The observer is formulated as:

$$\begin{cases} \epsilon = \hat{\xi}_1 - \mathbf{s}'_k \\ \dot{\hat{\xi}}_1 = \hat{\xi}_2 - \beta_1 \text{fal}(\epsilon, \alpha_1, \delta_1) + \mathbf{B} \mathbf{u}_k \\ \dot{\hat{\xi}}_2 = -\beta_2 \text{fal}(\epsilon, \alpha_2, \delta_2), \end{cases} \quad (16)$$

where  $\hat{\xi}_1, \hat{\xi}_2, \mathbf{B}$  represent the observed system states, the estimated total disturbance and the nominal system input matrix, respectively.  $\beta_1, \beta_2$  are the gain parameters. The nonlinear function is defined piecewise:

$$\text{fal}(\epsilon, \alpha, \delta) = \begin{cases} |\epsilon|^\alpha \text{sgn}(\epsilon), & |\epsilon| > \delta \\ \frac{\epsilon}{\delta^{1-\alpha}}, & |\epsilon| \leq \delta, \end{cases} \quad (17)$$

where  $0 < \alpha < 1$  governs the nonlinearity strength and influences the convergence rate, and  $\delta$  is the linear interval threshold.

Using the current state estimate  $\hat{\xi}_1$  as the initial condition, the NMPC optimizes a sequence of control inputs  $\{\mathbf{u}_k, \dots, \mathbf{u}_{k+N_p-1}\}$  over prediction horizon  $N_p$  by minimizing a cost function:

$$\min_{\mathbf{u}_k, \dots, \mathbf{u}_{k+N_p-1}} \left\| \mathbf{s}'_{k+N_p} - \mathbf{s}'_d \right\|_{\mathbf{P}}^2 + \sum_{i=k}^{k+N_p-1} \|\mathbf{u}_i\|_{\mathbf{R}}^2 \quad (18a)$$

$$\text{s.t. } \mathbf{s}'_{i+1} = f(\mathbf{s}'_i, \mathbf{u}_i) \quad (18b)$$

$$\mathbf{s}_{\min} \leq \mathbf{s}_i \leq \mathbf{s}_{\max} \quad (18c)$$

$$\mathbf{u}_{\min} \leq \mathbf{u}_i \leq \mathbf{u}_{\max} \quad (18d)$$

$$\Delta \mathbf{u}_{\min} \leq \mathbf{u}_i - \mathbf{u}_{i-1} \leq \Delta \mathbf{u}_{\max} \quad (18e)$$

$$Z_i > Z_{\text{safe}} \quad (18f)$$

where  $\mathbf{s}'_d$  is the desired terminal state;  $\mathbf{P}, \mathbf{R}$  are positive definite weighting matrices for terminal state error and control effort;  $\mathbf{s}_{\min}, \mathbf{s}_{\max}$  are the visibility constraints of FOV;  $\mathbf{u}_{\min}, \mathbf{u}_{\max}$  are the lower and upper bounds for velocity;  $\Delta \mathbf{u}_{\min}, \Delta \mathbf{u}_{\max}$  are the lower and upper bounds for velocity variation;  $Z_{\text{safe}}$  is the depth constraint that ensures docking safety. The first optimal control input  $\mathbf{u}_k^*$  from the NMPC solution is then converted to chassis commands  $\mathbf{u}_R^*$  by the mapping defined in (2) for execution.

## VI. EXPERIMENTS

### A. Experiments Setup



Fig. 4. Hardware platform of experiments, with key dimensions illustrated.

TABLE I  
PERFORMANCE COMPARISON

Method	$E_p \downarrow$		$E_s \downarrow$		$M_{sm} \downarrow$	
	$e_n[\text{cm}]$	$e_t[\text{cm}]$	$e_z[\text{cm}]$	$e_\theta[\text{degree}]$	$e_p[\text{pixel}]$	$v[\text{m/s}]$ $\omega[\text{m/s}]$
IBVS	5.410	31.827	<b>1.185</b>	12.375	1.834	0.011 <b>0.003</b>
MPC	2.604	0.764	2.601	4.559	44.599	0.064 0.204
Ours	<b>1.431</b>	<b>0.598</b>	1.429	<b>0.240</b>	<b>1.476</b>	<b>0.010</b> 0.057

As shown in Fig. 4, the key dimensions of robot's actuator and the trolley impose demands on the docking precision. We design the marker array by 4 high-power IR LEDs (3W output, 60° beam angle) with a constant-current driver, maintaining stable illumination. For visual perception, we employ a MV-SUA133GM industrial camera with 120° FOV providing 1280×1024 resolution. Due to the addition of the filter in camera, visible light can hardly pass through. Therefore, we employ a 940 nm light source to illuminate the calibration board, enabling convenient and efficient calibration. Each robot is equipped with an Intel NUC (Core

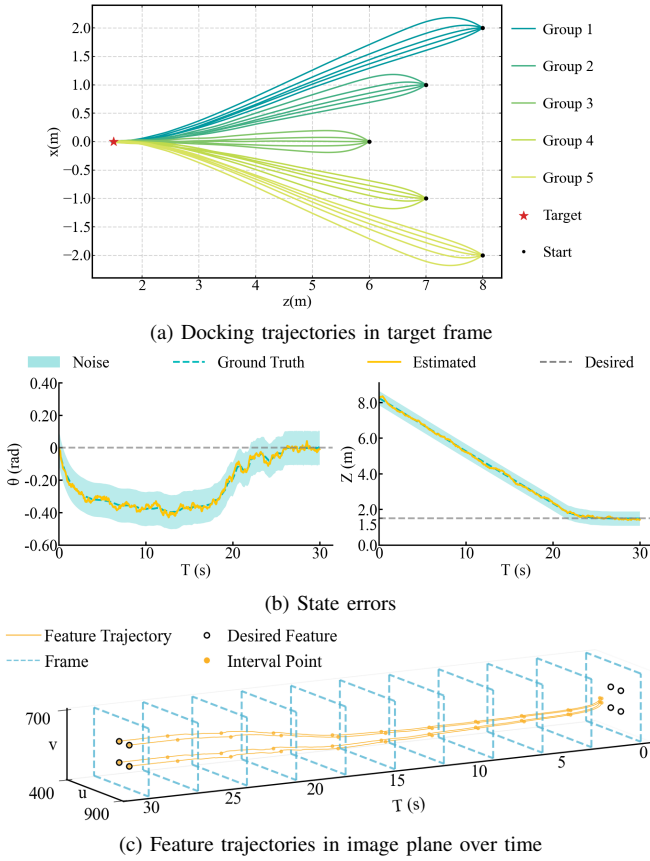


Fig. 5. Simulation results. (a) Follower robot trajectories. (b) Orientation and depth data for 3rd trajectory, with 2 standard deviation range marked as the shaded area. (c) Feature points motion in the image for the 3rd trajectory.

i7-1165G7 CPU@4.70GHz, 32GB RAM) for onboard computation. The software system is deployed on Ubuntu 20.04 with ROS2 Galactic, where the control problem is formulated using CasADi [28] and solved in real time by the IPOPT solver. Through node synchronization, this implementation maintains a 60 Hz perception frequency while achieving a 20 Hz control frequency.

We present comprehensive experimental validation of the proposed docking control method through both simulation and real-world implementations. The docking performance is quantitatively evaluated using the following metrics:

1)  $E_p$  - Error between the terminal and the desired position of the Follower robot, composed of the normal docking error  $e_n$  and tangential docking error  $e_t$ , with  $e_n = |z_{end}^T - z_d^T|$ ,  $e_t = |x_{end}^T - x_d^T|$ , where  $x_{end}^T$ ,  $z_{end}^T$  and  $x_d^T$ ,  $z_d^T$  denote the terminal and desired position in target frame  $\{T\}$ , respectively.

2)  $E_s$  - Error between the terminal and desired system states, including  $e_z$ ,  $e_\theta$  and  $e_p$ , with  $e_z = |Z_{end} - Z_d|$ ,  $e_\theta = |\theta_{end} - \theta_d|$ , which represent the depth and angular deviation between the terminal and desired states.  $e_p$  denotes the root mean square (RMS) distance error of  $n$  feature points in pixel frame  $\{P\}$ , calculated as:  $e_p = \sqrt{\frac{1}{n} \|\mathbf{p}_{end} - \mathbf{p}_d\|^2}$ , where  $\mathbf{p}_{end}$  and  $\mathbf{p}_d$  are terminal and desired coordinate vectors.

3)  $M_{sm}$  - Smoothness of the docking motion, calculated by the RMS of the velocity variation  $\Delta \mathbf{u} = [\Delta v, \Delta w]^T$

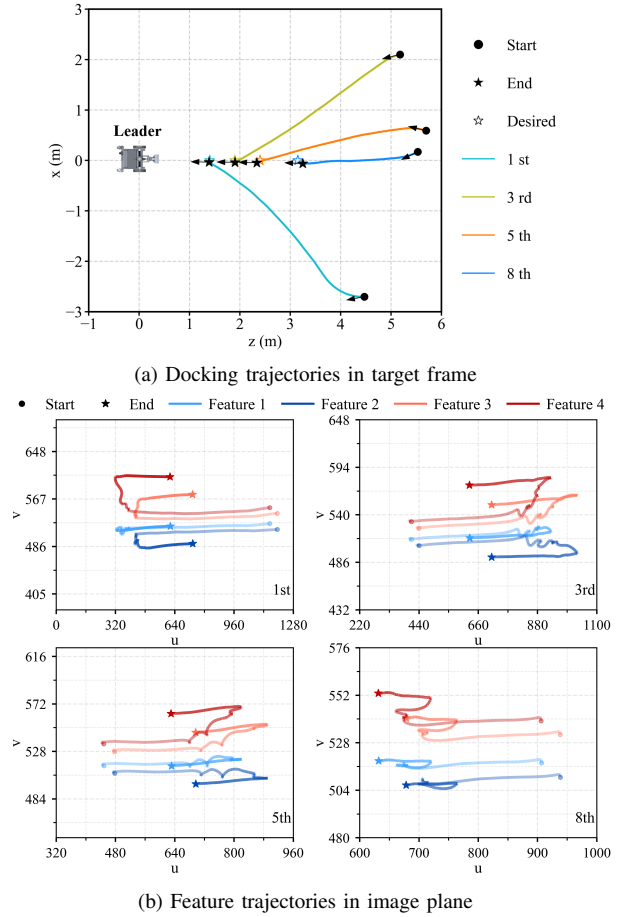


Fig. 6. Quantitative results of sequentially docking tasks. (a) Four docking trajectories (1st, 3rd, 5th, and 8th trolley) from different initial poses. Achieved terminal positions (black stars) are compared with desired docking positions (hollow stars). (b) Corresponding feature trajectories projected onto the pixel plane.

in each trial:  $M_{sm} = \sqrt{\frac{1}{T_{task}} \sum_{t=0}^{T_{task}} \Delta \mathbf{u}^2}$ , where  $T_{task}$  denotes the task execution time for docking control.

## B. Simulation Results

To validate the proposed control method, we conduct 25 simulation trials, organized into 5 groups based on initial position:  $(z_{init}, x_{init}) \in \{(8, 2), (7, 1), (6, 0), (7, -1), (8, -2)\}$  (defined in frame  $\{T\}$ ) with each position tested with 5 different initial orientations:  $\theta_{init} \in \{-35^\circ, -17.5^\circ, 0^\circ, 17.5^\circ, 35^\circ\}$ . The desired docking position is  $(1.5, 0)$  while the Leader remained stationary at  $(0, 0)$ . The simulation parameters precisely match physical hardware specifications, including camera intrinsics and installation height. We model realistic sensor noise by injecting Gaussian noise with  $\sigma(s) = [0.001, 0.001]^T$  for feature points,  $\sigma(Z) = 0.2$  m for depth estimation, and  $\sigma(\theta) = \pi/60$  rad for relative orientation, with each trial lasting 30 seconds.

Fig. 5 (a) demonstrates successful convergence to the desired pose from various initial conditions, validating the method's robustness. For detailed analysis, we examine the 3rd trajectory in Group 1 ( $\theta_{init} = 0^\circ$ ) as a representative case. Fig. 5 (b)-(c) present key state variables of the cho-

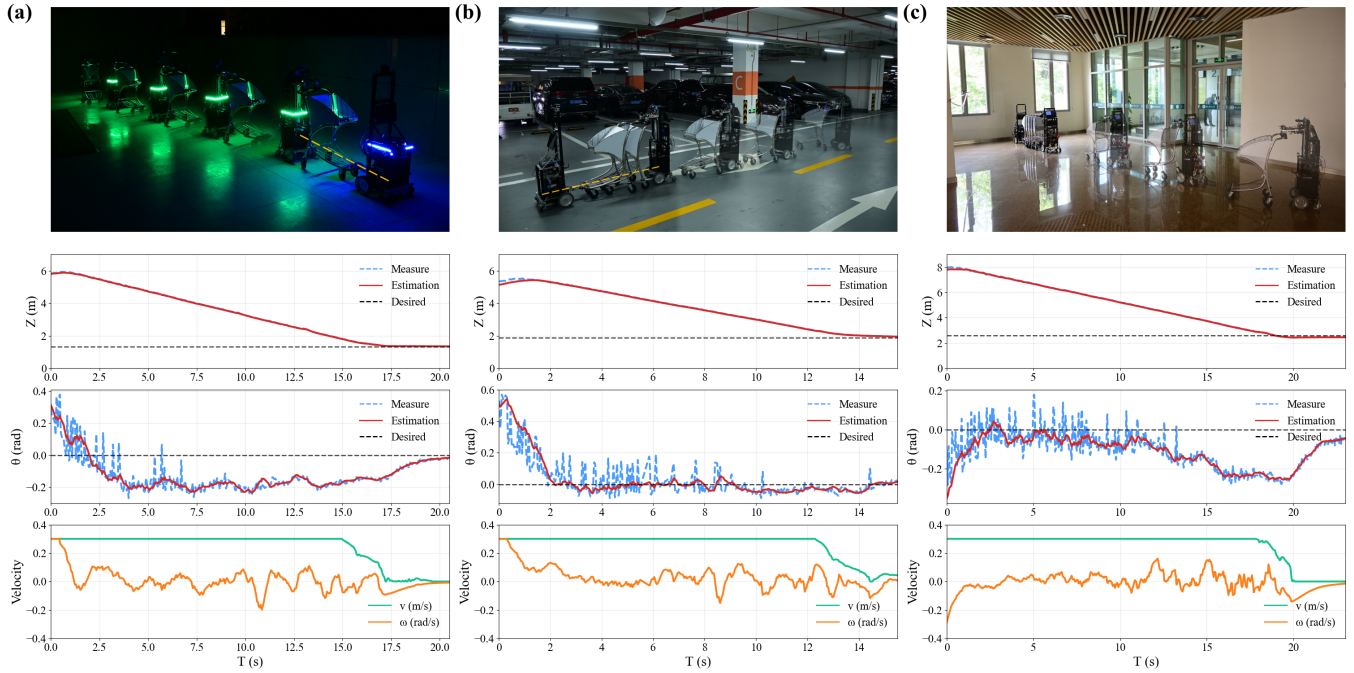


Fig. 7. Deployment results under varying environmental conditions: (a) dark outdoors, (b) underground parking lot with lighting variation, and (c) interior featuring glass wall. Collected data includes depth, angle variation and system output.

TABLE II  
DOCKING ERROR METRICS

	$e_n$ (cm)	$e_t$ (cm)	$e_\theta$ (degree)	$e_p$ (pixel)
avg $\pm$ std	1.31 $\pm$ 1.49	4.45 $\pm$ 1.74	2.16 $\pm$ 0.64	5.27 $\pm$ 0.83

sen case, confirming that the proposed observer maintains accurate state estimation throughout the docking maneuver despite motion disturbances.

Table I presents comparative experiments between the proposed method and other methods. All metrics are averaged over multiple trials with absolute errors. It demonstrates that the basic IBVS approach in [21] drives the robot toward the target by aligning the feature points with the desired points. However, due to nonholonomic constraints, the controller cannot decouple angular velocity commands that satisfy docking requirements. This results in accumulating orientation errors, leading to significant steady-state positioning deviations. The MPC method proposed in [24] tends to drive the robot near the target first before adjusting its orientation, resulting in discontinuous control outputs and trajectories, while also failing to ensure proper alignment of the feature points under noise. In contrast, the proposed method incorporates orientation as a state variable, enabling the robot to actively adjust its orientation during docking process, which satisfies multiple docking performance metrics while simultaneously achieving smooth outputs.

### C. Real-World Experiments

1) *Experiment 1 - Trolley docking*: To validate the effectiveness of the proposed method, we conduct experiments in a 6 m  $\times$  6 m area equipped with a motion capture system (0.1 mm accuracy) for real-time tracking of the Follower's trajectory and ground truth reference. To evaluate docking

accuracy, the Follower robot executes 25 docking trials in total from randomized initial configurations to sequentially dock the 1st-8th trolley.

We select several representative docking trials for visualization in Fig. 6 (a). The 1st and 3rd trolley docking trials are conducted with challenging initial configurations featuring significant lateral offsets (X-axis displacement in frame  $\{T\}$ ). For the 5th and 8th trolley docking tasks, despite progressively constrained operating space due to queue elongation, the Follower robot consistently achieved precise docking. Fig. 6 (b) shows that the feature points do not directly converge toward desired coordinates as basic IBVS, but are jointly optimized with other state variables, ensuring effective orientation adjustment for nonholonomic-constrained robot. As summarized in Table II, the error analysis provides performance metrics including means and variances. The critical parameters for successful docking: lateral position error  $e_t$  and angular alignment error  $e_\theta$ , demonstrated mean values of 4.45 cm and 2.16° respectively, achieving the required docking precision.

2) *Experiment 2 - Multi-environment*: To validate the performance of the system in real-world environments, we design 3 sets of trolley docking experiments under various conditions. The snapshots and corresponding data are presented in Fig. 7. Note that no sensors other than the proposed vision system are employed in experiments.

In dark outdoor environments, non-active visual features cannot be detected and extracted. An initial lateral error of ( $\approx$  2m) was intentionally set for docking the first trolley. After 2s, the orientation error ( $\theta$ ) gradually increases and then converges to 0, which matches the simulation results and demonstrates the capability of our method in handling



nonholonomic constraints. The second docking experiment is conducted in an underground parking lot. The system maintained successful docking performance for the 2nd trolley despite dynamically flickering lighting and irregular terrain surfaces. Finally, the docking experiment of the 5th trolley is performed near the sunlight-transmitting windows, reflective floor and glass partitions, starting from an initial depth of 8m. It demonstrate that the system maintains stable operation despite environmental light interference. The experimental data indicate that when two robots are at a long distance, the detection module exhibits significant noise in angle measurement. However, the system demonstrates strong resilience to angular fluctuations, confirming the effectiveness of the proposed disturbance rejection strategy.

## VII. CONCLUSIONS

This paper presents a monocular vision-based robotic docking system for reliable trolley collection in complex environments. By integrating active infrared feature with visual predictive control, our approach achieves millimeter-level docking accuracy while addressing the challenges of nonholonomic constraints, environmental variability and disturbances. We validate the system in diverse real-world settings, including dark outdoor areas and underground parking lots under various lighting and layout conditions. This work advances the practical deployment of autonomous logistics robots in unstructured public spaces. Future work will explore vision-based whole-body control and cooperative trolley transportation system, leveraging accelerated computing for improving real-time performance.

## REFERENCES

- [1] J. Scholz, S. Chitta, B. Marthi, and M. Likhachev, "Cart pushing with a mobile manipulation system: Towards navigation with moveable objects," in *2011 IEEE International Conference on Robotics and Automation*, 2011, pp. 6115–6120.
- [2] Y. Tang, M. Wisse, and W. Pan, "Unwieldy object delivery with nonholonomic mobile base: A free pushing approach," *IEEE Robotics and Automation Letters*, vol. 9, no. 10, pp. 8991–8998, 2024.
- [3] P. Xie, B. Xia, A. Hu, Z. Zhao, L. Meng, Z. Sun, X. Gao, J. Wang, and M. Q.-H. Meng, "Autonomous multiple-trolley collection system with nonholonomic robots: Design, control, and implementation," *Journal of Field Robotics*, vol. 42, no. 1, pp. 20–36, 2025.
- [4] Z. Zhang, P. Xie, Z. Sun, B. Xia, B.-K. Zhu, and J. Wang, "Integrating maneuverable planning and adaptive control for robot cart-pushing under disturbances," *arXiv preprint arXiv:2506.18410*, 2025.
- [5] C. Li, B. Li, R. Wang, and X. Zhang, "A survey on visual servoing for wheeled mobile robots," *International Journal of Intelligent Robotics and Applications*, vol. 5, no. 2, pp. 203–218, 2021.
- [6] Y. Wang, M. Shan, Y. Yue, and D. Wang, "Autonomous Target Docking of Nonholonomic Mobile Robots Using Relative Pose Measurements," *IEEE Transactions on Industrial Electronics*, vol. 68, no. 8, pp. 7233–7243, Aug. 2021.
- [7] G. Niu, Q. Yang, Y. Gao, and M.-O. Pun, "Vision-based autonomous landing for unmanned aerial and ground vehicles cooperative systems," *IEEE Robotics and Automation Letters*, vol. 7, no. 3, pp. 6234–6241, 2022.
- [8] E. Olson, "AprilTag: A robust and flexible visual fiducial system," in *2011 IEEE International Conference on Robotics and Automation*, May 2011, pp. 3400–3407.
- [9] B. Xia, H. Luan, Z. Zhao, X. Gao, P. Xie, A. Xiao, J. Wang, and M. Q.-H. Meng, "Collaborative Trolley Transportation System with Autonomous Nonholonomic Robots," in *2023 IEEE/RSJ International Conference on Intelligent Robots and Systems (IROS)*. Detroit, MI, USA: IEEE, Oct. 2023, pp. 8046–8053.
- [10] E. Tsiogas, I. Kleitsiotis, I. Kostavelis, A. Kargakos, D. Giakoumis, M. Bosch-Jorge, R. J. Ros, R. L. Tarazón, S. Likothonassis, and D. Tzovaras, "Pallet detection and docking strategy for autonomous pallet truck agv operation," in *2021 IEEE/RSJ International Conference on Intelligent Robots and Systems (IROS)*, 2021, pp. 3444–3451.
- [11] S. F. C. Gutierrez, M. Watanabe, M. Ooyama, T. Yamada, T. Yamada, N. Toshiki, S. Yamane, J. V. S. Luces, A. A. Ravankar, and Y. Hirata, "Real-time geometric-registration-based precision localization for autonomous docking in unstructured factory environment," *IEEE Robotics and Automation Letters*, vol. 10, no. 7, pp. 7198–7205, 2025.
- [12] P. Wang, C. Wang, J. Wang, and M. Q.-H. Meng, "Quadrotor autonomous landing on moving platform," *Procedia Computer Science*, vol. 209, pp. 40–49, 2022, proceedings of the 2022 International Symposium on Biomimetic Intelligence and Robotics (ISBIR).
- [13] Z. Cao, L. Zhang, R. Xu, C. Liu, B. Lin, X. Ji, and H. Qian, "Design of a self-correctable docking mechanism in disturbed water surface environment," *IEEE Robotics and Automation Letters*, vol. 9, no. 11, pp. 9773–9780, 2024.
- [14] D. Herrero, J. Villagrà, and H. Martínez, "Self-Configuration of Waypoints for Docking Maneuvers of Flexible Automated Guided Vehicles," *IEEE Transactions on Automation Science and Engineering*, vol. 10, no. 2, pp. 470–475, Apr. 2013.
- [15] J. Peng, Z. Liao, H. Yao, Z. Su, Y. Zeng, and H. Dai, "Mpc-based human-accompanying control strategy for improving the motion coordination between the target person and the robot," in *2023 IEEE/RSJ International Conference on Intelligent Robots and Systems (IROS)*. IEEE, 2023, pp. 7969–7975.
- [16] M. Yadegar, Z. Kashi, H. Ghaderi, N. Meskin, and M. Noorizadeh, "Autonomous Target Docking With Obstacle Avoidance and Final Velocity Control for Non-Holonomic Mobile Robots," *IEEE Transactions on Automation Science and Engineering*, vol. 22, pp. 4039–4050, 2025.
- [17] Y. Chen, D. F. Paez-Granados, B. Leme, and K. Suzuki, "Virtual landmark-based control of docking support for assistive mobility devices," *IEEE/ASME Transactions on Mechatronics*, vol. 26, no. 4, pp. 2007–2015, 2021.
- [18] Y. Zheng, C. Zheng, J. Shen, P. Liu, and S. Zhao, "Keypoint-Guided Efficient Pose Estimation and Domain Adaptation for Micro Aerial Vehicles," *IEEE Transactions on Robotics*, vol. 40, pp. 2967–2983, 2024.
- [19] Z. Lu, Y. Wu, S. Yang, K. Zhang, and Q. Quan, "Fast and Omnidirectional Relative Position Estimation With Circular Markers for UAV Swarm," *IEEE Transactions on Instrumentation and Measurement*, vol. 73, pp. 1–11, 2024.
- [20] Z. Xun, J. Huang, Z. Li, Z. Ying, Y. Wang, C. Xu, F. Gao, and Y. Cao, "CREPES: Cooperative RELative Pose Estimation System," in *2023 IEEE/RSJ International Conference on Intelligent Robots and Systems (IROS)*. Oct. 2023, pp. 5274–5281.
- [21] F. Chaumette, S. Hutchinson, and P. Corke, *Visual Servoing*. Cham: Springer International Publishing, 2016, pp. 841–866.
- [22] E. Malis, F. Chaumette, and S. Boudet, "2 1/2 D visual servoing," *IEEE Transactions on Robotics and Automation*, vol. 15, no. 2, pp. 238–250, Apr. 1999.
- [23] J. Ernesto Solanes, L. Armesto, J. Tornero, and V. Gírbés, "Improving image-based visual servoing with reference features filtering," in *2013 IEEE International Conference on Robotics and Automation*, 2013, pp. 3083–3088.
- [24] F. Ke, Z. Li, H. Xiao, and X. Zhang, "Visual Servoing of Constrained Mobile Robots Based on Model Predictive Control," *IEEE Transactions on Systems, Man, and Cybernetics: Systems*, vol. 47, no. 7, pp. 1428–1438, Jul. 2017.
- [25] G. Allibert, E. Courtial, and F. Chaumette, "Predictive Control for Constrained Image-Based Visual Servoing," *IEEE Transactions on Robotics*, vol. 26, no. 5, pp. 933–939, Oct. 2010.
- [26] Z. Jin, J. Wu, A. Liu, W.-A. Zhang, and L. Yu, "Gaussian process-based nonlinear predictive control for visual servoing of constrained mobile robots with unknown dynamics," *Robotics and Autonomous Systems*, vol. 136, p. 103712, Feb. 2021.
- [27] T. Collins and A. Bartoli, "Infinitesimal Plane-Based Pose Estimation," *International Journal of Computer Vision*, vol. 109, no. 3, pp. 252–286, Sep. 2014.
- [28] J. A. E. Andersson, J. Gillis, G. Horn, J. B. Rawlings, and M. Diehl, "CasADi – A software framework for nonlinear optimization and optimal control," *Mathematical Programming Computation*, vol. 11, no. 1, pp. 1–36, 2019.